Quantum of optical absorption in two-dimensional semiconductors

Hui Fang[a,b,c], Hans A. Bechtel[d], Elena Plis[e], Michael C. Martin[d], Sanjay Krishna[e], Eli Yablonovitch[a,b,1], and Ali Javey[a,b,c,1]

[a]Department of Electrical Engineering and Computer Sciences, University of California, Berkeley, CA 94720; [b]Materials Sciences Division, Lawrence Berkeley National Laboratory, Berkeley, CA 94720; [c]Berkeley Sensor and Actuator Center, University of California, Berkeley, CA 94720; [d]Advanced Light Source Division, Lawrence Berkeley National Laboratory, Berkeley, CA 94720; and [e]Center for High Technology Materials, University of New Mexico, Albuquerque, NM 87106

Contributed by Eli Yablonovitch, May 26, 2013 (sent for review February 11, 2013)

The optical absorption properties of free-standing InAs nanomembranes of thicknesses ranging from 3 nm to 19 nm are investigated by Fourier transform infrared spectroscopy. Stepwise absorption at room temperature is observed, arising from the interband transitions between the subbands of 2D InAs nanomembranes. Interestingly, the absorptance associated with each step is measured to be ∼1.6%, independent of thickness of the membranes. The experimental results are consistent with the theoretically predicted absorptance quantum, $A_Q = \pi\alpha/n_c$ for each set of interband transitions in a 2D semiconductor, where α is the fine structure constant and n_c is an optical local field correction factor. Absorptance quantization appears to be universal in 2D systems including III–V quantum wells and graphene.

The optical properties of heterostructure quantum wells (QWs) have been extensively studied since the 1970s, in GaAs/AlGaAs (1), GaInAs/AlInAs (2, 3), InGaAs/InP (4), and HgCdTe/CdTe (5). Here we do a careful quantitative examination of the intrinsic absorption properties of free-standing 2D semiconductor thin films, which has previously been done only for layered structures, such as MoS_2 (6). (The criterion of real two-dimensionality is that the material thickness be smaller than the electron Bohr radius.)

Previous work has shown that graphene, a 2D semimetal, has a universal value of light absorption, namely $\pi\alpha$, where α is the fine structure constant (7). Here, we use free-standing InAs membranes with exceptionally small thickness as a model material system to accurately probe the absorption properties of 2D semiconductors as a function of thickness. We demonstrate that the magnitude of the light absorption is an integer product of a quantum of absorptance. Specifically, each set of interband transitions between the 2D subbands results in a quantum unit of absorptance of $A_Q \sim \pi\alpha/n_c$, where n_c is the optical local field correction factor. The total absorptance for the first several sets of interband transitions is simply given as $A = MA_Q$, where M is the integer number of allowed transitions for a given photon energy. The result here appears to be universal, except for small correction factors associated with higher bands.

Recently, there has been a high level of interest in exploring the fundamental science (6–10) and associated devices (11–20) of free-standing (i.e., attached to a substrate by van der Waals or other weak forces) 2D semiconductors. Two-dimensional layered semiconductors [*e.g.*, MoS_2 (11), WSe_2 (15), GaSe (16), $Bi_2Sr_2CaCu_2O_x$ (17), Bi_2Se_3 (18), and Bi_2Te_3 (19) or diamond/zinc-blend structures InAs (12) and InGaSb (20)] can be readily mounted on virtually any support substrate, thereby enabling a wide range of novel device concepts and practical applications. In one example system, InAs quantum membranes (QMs) with adjustable thicknesses down to a few atomic layers have been realized by a layer transfer process onto a user-defined substrate (12). The approach enables the direct optical absorption studies of fully relaxed (i.e., unstrained) (21) 2D III–V semiconductors by using transparent substrates, without the constraints of the original growth substrate (10). Here, we use InAs membranes of thickness $L_z \sim$ 3–19nm on CaF_2 support substrates as a model material system for examining the absorption properties of 2D semiconductors. Given the large Bohr radius of ∼34 nm (22) in bulk InAs, strong quantum confinement of carriers is readily obtained for sub-20-nm quantum membrane thicknesses. Note that there are only ∼5 unit cells in a 3-nm-thick InAs QM, given its lattice constant of ∼0.6 nm (23). In such a quantum mechanically confined 2D system, there is electronic band dispersion in the two unconfined directions, with discrete energy subband edges at values determined by quantum confinement (24) in the third direction. In our case, the InAs QMs can be effectively treated as infinitely deep potential wells, because they are confined by air on one side and by a wide band-gap (25) CaF_2 substrate on the other side. Fig. 1*A* shows the optical microscope image of a periodic array of ∼5-μm-wide InAs strips (of ∼3 nm thickness), on a CaF_2 crystal substrate produced by the layer transfer process (*SI Text*). CaF_2 was chosen as the support substrate as it is optically transparent for the wavelength range of interest. From visual appearance (Fig. 1*A*), it is evident that ultrathin InAs QMs exhibit strong optical contrast, thereby allowing for the detailed optical characterization even for the films consisting of a few atomic layers in thickness.

Fig. 1*B* shows the calculated energy levels of a 9-nm InAs QM with CaF_2 and air boundaries. The molecular beam epitaxy-grown InAs samples are not intentionally doped, eliminating band filling (the Fermi level was calculated from an estimated bulk electron density of $2\times10^{16}/cm^3$) (26). Here, the effects of surface accumulation layers due to surface defects are ignored (see Fig. S1 for surface accumulation layer effects). Fig. 1*C* depicts the qualitative band structure of a 2D InAs QM, with vertical arrows indicating the interband transitions from the nth heavy hole (*hh*)/light hole (*lh*) subband to the nth electron (*e*) subband. Here we define e_n–hh_n and e_n–lh_n as the nth set of interband transitions. Due to spatial matching of electron/hole wave functions in different energy subbands, interband transitions in quantum wells are favored when $\Delta n = n' - n = 0$, where n' and n are the subband indexes for electrons and holes, respectively (27). Consequently, there are two allowed transitions to each electron subband: one from the corresponding *hh* subband and the other from *lh* subband.

We use Fourier transform infrared (FTIR) microspectroscopy (Fig. 2) to probe optical interband transitions (in the range 0.3 eV < $h\nu$ < 1.2 eV) in InAs QMs at room temperature (*SI Text*). Transmittance and reflectance spectra were collected in the range of 2,414–9,656 cm^{-1} (0.30–1.20 eV) over an aperture size of ∼50 × 50 μm^2, with 8 cm^{-1} (1 meV) resolution and 512

Author contributions: H.F. and A.J. designed research; H.F., H.A.B., M.C.M., E.Y., and A.J. performed research; H.F., H.A.B., E.P., M.C.M., S.K., and A.J. contributed new reagents/analytic tools; H.F., E.Y., and A.J. analyzed data; and H.F., E.Y., and A.J. wrote the paper.

The authors declare no conflict of interest.

Freely available online through the PNAS open access option.

[1]To whom correspondence may be addressed. E-mail: eliy@eecs.berkeley.edu or ajavey@eecs.berkeley.edu.

This article contains supporting information online at www.pnas.org/lookup/suppl/doi:10.1073/pnas.1309563110/-/DCSupplemental.

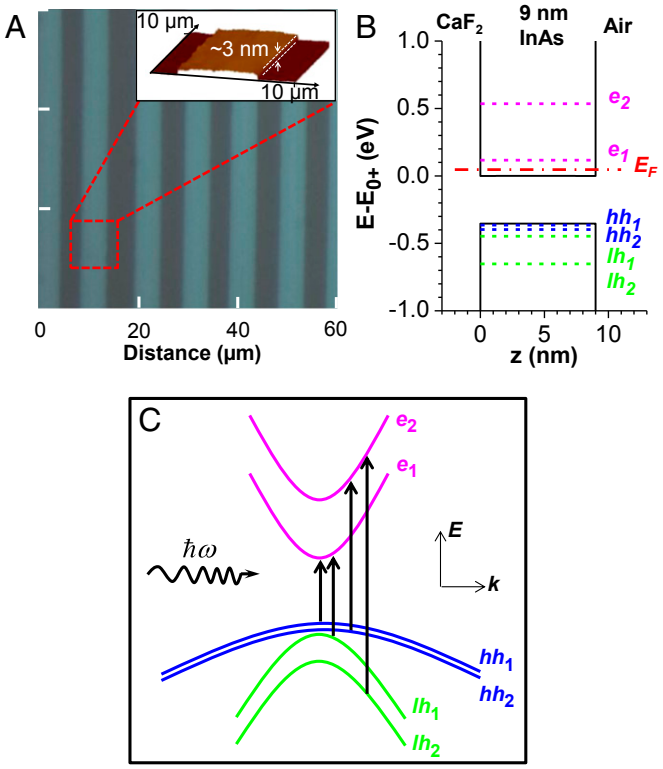

Fig. 1. (*A*) Optical microscope image of InAs 2D strips (~3 nm thick) on a CaF_2 substrate. (*Inset*) The atomic force microscope image of a single InAs strip. (*B*) CaF_2/InAs (9 nm)/air quantum well band diagram with energy referring to E(z = 0$^+$), abbreviated as E_{0+}. E_F shows the quasi-Fermi level, whereas e_1, e_2, hh_1, hh_2, lh_1, and lh_2 are the indexes for the conduction and valence subbands. Note that only the first two conduction/valence subband edges are shown. (*C*) Qualitative band structure schematic of a 2D InAs QM, with arrows indicating the allowed optical interband transitions between valence and conduction subbands.

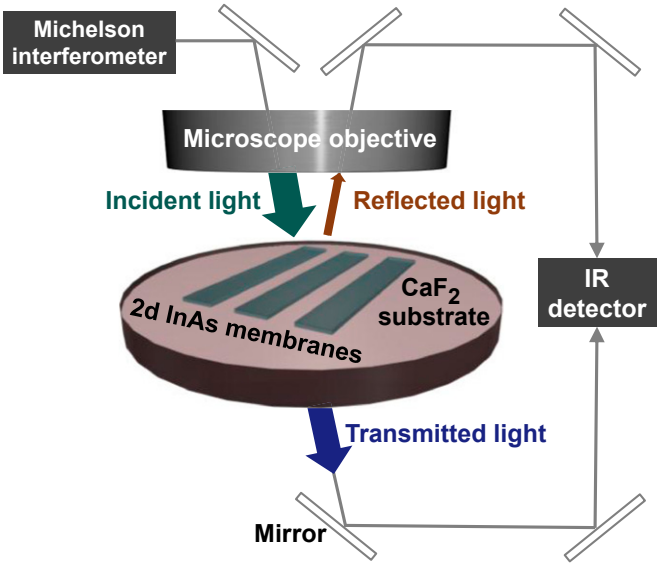

Fig. 2. Schematic illustration of the FTIR microspectroscopy setup used for the absorption measurements. The absorption spectrum is obtained from the measured transmission and reflection spectra. The incident light angle was actually perpendicular to the membrane.

averages for all samples with different thicknesses. Atmospheric H_2O and CO_2 effects were removed using OMNIC 8.2 software (Thermo Scientific). The absorption spectra of InAs QMs for each thickness were obtained by subtracting the transmittance and reflectance from a normalized 100% spectrum, yielding Fig. 3. The final spectra were generated by dividing the measured spectra by the fractional area fill factor of the InAs strips. Fig. 4 shows the overlaid absorptance (A) spectra of InAs QMs with $L_z \sim 3$ nm, 6 nm, 9 nm, 14 nm, and 19 nm. Clear step-like features are observed in the absorptance spectra arising from the quantized interband transitions between the 2D subbands (10). The spacings between the measured absorptance steps are in quantitative agreement with the calculated interband energy spacings (see Fig. S2 for the detailed analysis). Note that intersubband transitions are negligible due to our transverse electric (TE) polarization. The experimental finding here is that the individual absorptance steps plateau at ~1.6 ± 0.2% (SD) for all samples, regardless of the QM thickness. The result was reproducible for multiple samples and measurements.

To shed light on this observed absorption behavior, the electron–photon interaction in a semiconductor material is theoretically evaluated from Fermi's golden rule. If a light wave with electric field $\vec{E}$, polarization vector $\hat{e}$, and frequency ω is incident perpendicular to a direct band-gap semiconductor membrane with a thickness L_z, in an infinitely deep potential well model (28), the optical absorption coefficient is

$$\alpha'(\omega) = \frac{e^2}{n_r c \varepsilon_o m_o^2 \omega L_z \hbar^2} \frac{1}{1/m_{en}^* + 1/m_{hn}^*} \left| \hat{e} \cdot \vec{p}_{cv} \right|^2, \qquad [1]$$

which is a step function for each interband transition, where e is the electron charge, n_r is the real part of surrounding refractive index, c is the speed of light, ε_o is the vacuum permittivity, m_o is the free electron mass, $\hbar$ is Planck's constant, m_{en}^* and m_{hn}^* are

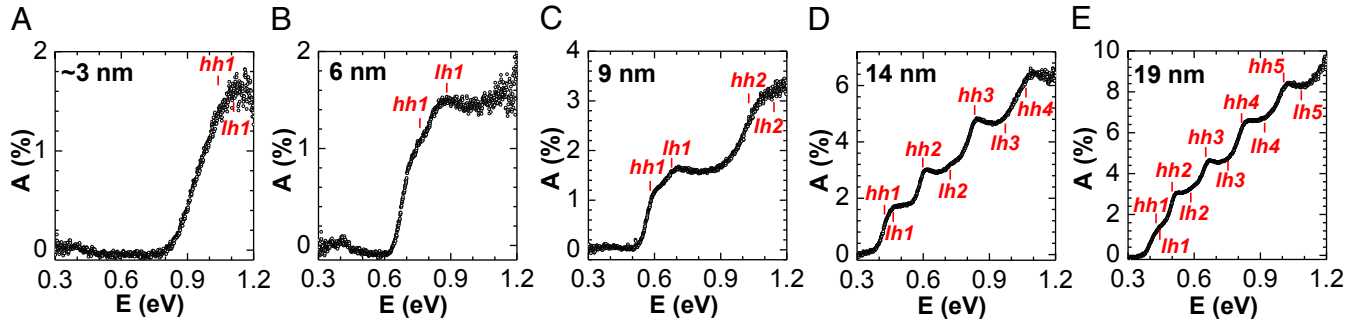

Fig. 3. Absorptance for (*A*) 3-nm, (*B*) 6-nm, (*C*) 9-nm, (*D*) 14-nm, and (*E*) 19-nm InAs quantum membranes. The absorptance spectra are corrected by dividing by the surface area fill factor of InAs.

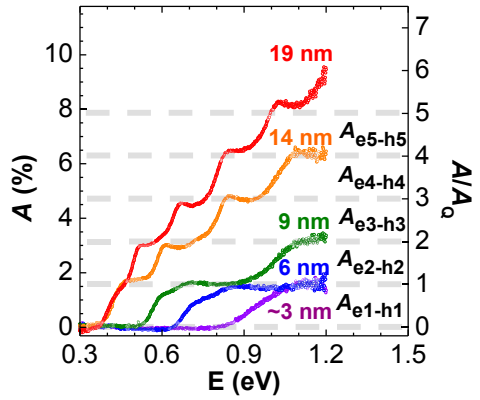

Fig. 4. Absorptance spectra of InAs QMs with thickness of $L_z \sim 3$ nm, 6 nm, 9 nm, 14 nm, and 19 nm at room temperature, showing universal absorptance steps of $A_Q \sim 1.6\%$ in magnitude. Dashed lines indicate each 1.6% of absorptance. The $A_{en\text{-}hn}$ represent the absorptance from the corresponding interband transitions, e_n–hh_n and e_n–lh_n.

the effective mass for electrons and holes of the nth conduction and valence subbands present from the 2D density-of-states, and $|\hat{e}\cdot\vec{p}_{cv}|^2$ is the momentum matrix element describing the electron–photon interaction. Eq. **1** arises from Fermi's Golden Rule, with optical perturbation $|e\vec{A}\cdot\vec{p}_{cv}/m_o|$, where $\vec{A}$ is the vector potential related to the optical electric field as $\vec{E} = j\omega\vec{A}$.

The reciprocal effective masses $1/m_c$ and $1/m_h$ arise in $k\cdot p$ perturbation theory (29) from a similar perturbation $\hbar|\vec{k}\cdot\vec{p}_{cv}/m_o|$. The reduced effective mass produced by this repulsion of conduction and valence bands in second-order $k\cdot p$ perturbation theory is $1/m^*_{en} + 1/m^*_{hn} = 4|p_{cv}/m_o|^2/\mathrm{E}_{cv}$, where $\mathrm{E}_{cv} = \hbar\omega$ is the interband transition energy.

Thus, $k\cdot p$ perturbation theory puts $|p_{cv}|^2$ in the denominator of Eq. **1**, whereas the optical perturbation puts $|p_{cv}|^2$ in the numerator of Eq. **1**. Thus, the momentum matrix element $|p_{cv}|^2$ cancels. Many of the other terms in Eq. **1** cancel as well, leaving behind the dimensionless absorptance $\alpha' L_z = \pi(e^2/4\pi\varepsilon_o\hbar c)/n_r$. Aside from π, and a correction for the surrounding refractive index n_r, the absorptance per 2D sublevel is $(e^2/4\pi\varepsilon_o\hbar c)$, a group of fundamental constants known as the fine structure constant $(e^2/4\pi\varepsilon_o\hbar c) = \alpha = 1/137$.

The prime on the absorption coefficient α' is meant to distinguish it from the fine structure constant α. Because $\alpha' L_z$ is dimensionless, it is somewhat inevitable that it would be related to α, the dimensionless parameter in opto-electronics and quantum physics. Indeed, optical absorption depends on electric charge, and α is actually electric charge squared (in fundamental units where $\hbar = 1$, $c = 1$, $4\pi\varepsilon_o = 1$).

The simplified calculation above is vindicated by Szkopek's detailed calculations (30, 31), which multiply the step function by a Sommerfeld Coulomb correction factor

$$S(\omega) = \frac{2}{1 + \exp\left\{-2\pi\sqrt{Ry/(\hbar\omega - \mathrm{E}_{cv})}\right\}},$$

where Ry is the electron-hole Rydberg binding energy. This puts a sharp, narrow, double-height spike, right at the step function, whose width is related to the typical millivolt hydrogenic binding energy. In the experiment (Fig. 4) the double-height spikes are washed out, and hardly seen, leaving only small vestigial peaks at each step.

There is an additional correction. The dimensionless absorption steps that we observe at ~1.6% are actually smaller than $\pi\alpha = 2.3\%$. This is due to a local optical electric field correction factor, which we call n_c. In a surrounding refractive index n_r, $n_c = n_r$, as is clear from Eq. **1**. When the quantum membrane film is mounted on a substrate of refractive index n, it experiences both the incident electric field, E_o, and the Fresnel reflected electric field $\{(1-n)/(1+n)\}E_o$. Superposing the incident and reflected fields, that local optical electric field at the quantum membrane is weaker by $\{2/(1+n)\}E_o$, which reduces the optical absorption by $\{2/(1+n)\}^2$, and the local field correction factor becomes $n_c = \{(n+1)/2\}^2$, yielding the corrected step absorption A_Q:

$$A_Q \equiv \alpha'_n(\omega)L_z = \frac{\pi\alpha}{n_c} = \pi\alpha\left(\frac{2}{1+n}\right)^2.$$

In our case the refractive index of CaF_2 is $n = 1.43$, changing the optical local field correction factor n_c to $\{(1+n)/2\}^2 = 1.48$, reducing the absorption step height to ~1.58%, in close agreement with our observed step height in Fig. 4.

Thus, we have shown experimentally and theoretically that light absorption in 2D semiconductors is independent of specific material parameters, such as band gap, effective mass, and thickness. The simplification of $A = M{\cdot}A_Q$ holds true over a broad range of photon energy, given that the considerable confinement energy shifts with M.

The measured absorptance values for previously reported III–V and II–VI heterostructure QWs are in the range of 0.6–1.1% per QW for the first step (1–5), slightly smaller than the A_Q value presented in this work. This is expected due to an optical local field correction factor $n_c \sim 3.5$, appropriate to a quantum well grown and embedded in high-index material, rather than to our case of free-standing quantum membrane on a low-index substrate. On the other hand, the result here is also consistent with the reported absorptance for graphene (7), $A \sim \pi\alpha$, which is for a totally suspended membrane with vacuum on either side.

In summary, light absorption in near-ideal 2D semiconductors is experimentally examined by using free-standing InAs QMs as a model material system. The absorptance of 2D InAs is found to be an integer multiple of the quantum absorptance, A_Q, governed only by the fundamental physical constant α. Besides its significance in the basic understanding of electron–photon interactions in quantum confined semiconductors, this result provides a unique insight toward the use of 2D semiconductors for novel photonic and optoelectronic devices. Future work should focus on experimental studies of the absorptance magnitude of other 2D material systems.

ACKNOWLEDGMENTS. This work was supported by the Director, Office of Science, Office of Basic Energy Sciences, Materials Sciences and Engineering Division of the US Department of Energy under Contract DE-AC02-05CH11231. A.J. and E.Y. acknowledge funding from the National Science Foundation (NSF) Center for Energy Efficient Electronics Science (NSF Award 0939514). A.J. acknowledges support from the World Class University program at Sunchon National University.

1. Dingle R, Wiegmann W, Henry CH (1974) Quantum states of confined carriers in very thin $Al_xGa_{1-x}As$-GaAs-$Al_xGa_{1-x}As$ heterostructures. *Phys Rev Lett* 33:827–830.
2. Masumoto Y, Matsuura M, Tarucha S, Okamoto H (1985) Direct experimental observation of two-dimensional shrinkage of the exciton wave function in quantum wells. *Phys Rev B Condens Matter* 32(6):4275–4278.
3. Stolz W, Maan JC, Altarelli M, Tapfer L, Ploog K (1987) Absorption spectroscopy on $Ga_{0.47}In_{0.53}As/Al_{0.48}In_{0.52}As$ multi-quantum-well heterostructures. II. Subband structure. *Phys Rev B Condens Matter* 36(8):4310–4315.
4. Skolnick MS, et al. (1987) InGaAs-InP multiple quantum wens grown by atmospheric pressure metaiorganic chemical vapor deposition. *Appl Phys Lett* 51(1):24–26.
5. Cesar CL, et al. (1990) Detailed characterization of HgCdTe/CdTe multiple quantum wells. *Appl Phys Lett* 56:283–285.
6. Mak KF, Lee C, Hone J, Shan J, Heinz TF (2010) Atomically thin MoS_2: A new direct-gap semiconductor. *Phys Rev Lett* 105(13):136805.
7. Nair RR, et al. (2008) Fine structure constant defines visual transparency of graphene. *Science* 320(5881):1308.

8. Splendiani A, et al. (2010) Emerging photoluminescence in monolayer MoS_2. *Nano Lett* 10(4):1271–1275.
9. Najmaei S, Liu Z, Ajayan PM, Lou J (2012) Thermal effects on the characteristic Raman spectrum of molybdenum disulfide (MoS_2) of varying thicknesses. *Appl Phys Lett* 100:013106.
10. Takei K, et al. (2011) Quantum confinement effects in nanoscale-thickness InAs membranes. *Nano Lett* 11(11):5008–5012.
11. Radisavljevic B, Radenovic A, Brivio J, Giacometti V, Kis A (2011) Single-layer MoS_2 transistors. *Nat Nanotechnol* 6(3):147–150.
12. Ko H, et al. (2010) Ultrathin compound semiconductor on insulator layers for high-performance nanoscale transistors. *Nature* 468(7321):286–289.
13. Li H, et al. (2012) Fabrication of single- and multilayer MoS_2 film-based field-effect transistors for sensing NO at room temperature. *Small* 8(1):63–67.
14. Liu H, Ye PD (2012) MoS_2 dual-gate MOSFET with atomic-layer-deposited Al_2O_3 as top-gate dielectric. *IEEE Elec Dev Lett* 33:546–548.
15. Fang H, et al. (2012) High-performance single layered WSe_2 p-FETs with chemically doped contacts. *Nano Lett* 12(7):3788–3792.
16. Hu P, Wen Z, Wang L, Tan P, Xiao K (2012) Synthesis of few-layer GaSe nanosheets for high performance photodetectors. *ACS Nano* 6(7):5988–5994.
17. Novoselov KS, et al. (2005) Two-dimensional atomic crystals. *Proc Natl Acad Sci USA* 102(30):10451–10453.
18. Cho S, Butch NP, Paglione J, Fuhrer MS (2011) Insulating behavior in ultrathin bismuth selenide field effect transistors. *Nano Lett* 11(5):1925–1927.
19. Teweldebrhan D, Goyal V, Balandin AA (2010) Exfoliation and characterization of bismuth telluride atomic quintuples and quasi-two-dimensional crystals. *Nano Lett* 10(4):1209–1218.
20. Takei K, et al. (2012) Nanoscale InGaSb heterostructure membranes on Si substrates for high hole mobility transistors. *Nano Lett* 12(4):2060–2066.
21. Fang H, et al. (2011) Strain engineering of epitaxially transferred, ultrathin layers of III-V semiconductor on insulator. *Appl Phys Lett* 98:012111.
22. Efros AL, Rosen M (2000) The electronic structure of semiconductor nanocrystals. *Annu Rev Mater Sci* 30:475–521.
23. Mikhailova MP (1996) *Handbook Series on Semiconductor Parameters* (World Scientific, London), Vol 1.
24. Ando T, Fowler B, Stern F (1982) Electronic properties of two-dimensional systems. *Rev Mod Phys* 54:437–672.
25. Poole RT, et al. (1975) Electronegativity as a unifying concept in the determination of fermi energies and photoelectric thresholds. *Chem Phys Lett* 36:401–403.
26. Noguchi M, Hirakawa K, Ikoma T (1991) Intrinsic electron accumulation layers on reconstructed clean InAs(100) surfaces. *Phys Rev Lett* 66(17):2243–2246.
27. Fox M (2001) *Optical Properties of Solids* (Oxford Univ Press, New York).
28. Chuang SL (2009) *Physics of Photonic Devices* (Wiley, Hoboken, NJ), 2nd Ed.
29. Davies JH (1997) *The Physics of Low-Dimensional Semiconductors: An Introduction* (Cambridge Univ Press, New York), 1st Ed.
30. Szkopek T (2011) Optical frequency conductance, susceptance and admittance of quantum wells. *IEEE J Quantum Electron* 47:500–509.
31. Yoshita M, Kamide K, Suzuura H, Akiyama H (2012) Applicability of continuum absorption in semiconductor quantum wells to absolute absorption-strength standards. *Appl Phys Lett* 101:032108.

Supporting Information

Fang et al. 10.1073/pnas.1309563110

SI Text

Fabrication of 2D InAs Membranes. InAs thin films (thicknesses of 7 nm, 10 nm, 15 nm, and 20 nm) were grown by molecular beam epitaxy on a GaSb handling wafer with an AlGaSb (60 nm thickness) sacrificial layer. The InAs layer was pattern etched into microribbon strips with a photoresist mask (~10 μm pitch and ~5 μm line width), using a mixture of citric acid (1 g/mL water) and hydrogen peroxide (30%) at 1:20 vol ratio. After selective etching of the AlGaSb layer with ammonium hydroxide [3% (vol/vol) in water], the InAs membranes were transferred onto CaF_2 substrates (International Crystal Laboratories; double side polished, 1 mm thick), using polydimethylsiloxane substrates (~2 mm thick). The photoresist was then removed with acetone. The final InAs thicknesses after transfer were 6 nm, 9 nm, 14 nm, and 19 nm ± 1 nm as confirmed by transmission electron microscopy (1, 2). To obtain the 3 ± 1-nm-thick InAs sample, a 6-nm InAs membrane on CaF_2 was etched alternately by citric acid and hydrogen peroxide.

FTIR Measurements. The light absorption of 2D InAs quantum membranes (QMs) (L_z = 3–19 nm) was measured by Fourier transform infrared (FTIR) microspectroscopy, using a Thermo Scientific Nicolet Continuμm Infrared Microscope with a Nicolet 6700 FTIR spectrometer (beamsplitter: CaF_2) at Beamlines 1.4 and 5.4 at the Advanced Light Source. We note that the same FTIR setup has been successfully used by Wang et al. (3, 4) with down to a few percent accuracy to measure monolayer and bilayer graphene, where the absorption magnitude has been established both experimentally and theoretically (5).

Surface Charge Effects on the Band Diagram. The InAs epilayers are not intentionally doped. A body doping concentration (N_D) of 2×10^{16} cm^{-3} was assumed to construct the band diagrams of those InAs 2D quantum wells. Note that this N_D value is in close agreement with our previous device simulation fitting of electrical measurements on similar membranes (1, 6). Bulk InAs is known to form polar surfaces with positive surface charges due to defects and an electron accumulation layer in the near surface region. This may affect the shape of the quantum potential well. We modeled these effects. The surface defect states (unoccupied In adatoms states) are found to be above the conduction band minimum (CBM) with a density of ~10^{12} cm^{-2} (7–10). Fig. S1 shows the energy band diagrams of different thickness InAs QMs for the cases without and with surface charges ($N_S = 10^{12}$ cm^{-2}). The results are simulated by solving Poisson's equation and Schrodinger's equation self-consistently, using a next-nano^3 simulator.

Comparison of Interband Transition Energies Between Experiments and Modeling. Fig. S2 presents the experimental interband transition energies along with those obtained from simulation, with and without surface charges. To determine the experimental interband transition energies from the absorption spectra, the first derivatives were obtained, where the location of each peak corresponds to the energy of an interband transition. For the theoretical modeling with surface accumulation charges ($N_S = 10^{12}$ cm^{-2}), the transition energies for $E_{en\text{-}hhn}$ were taken as $E_F - E_{hhn}$ if E_F is above E_{en}. As depicted in Fig. S2, the effect of surface charges (i.e., E_F position) is minimal and only the onset of absorption for the first interband transition is shifted slightly. The experimental values fall between the two modeling cases, closer to the case where there is no N_S.

Intersubband Transitions. The absorption from intersubband transitions is expected to be negligible for our measurement configuration using TE polarized light, where the light wave vector is perpendicular to the QMs. The reason is that the intersubband dipole moment $\vec{\mu}_{ba} = \langle \psi_b | e\vec{r} | \psi_a \rangle$ is z-polarized due to the spatial confinement in the z direction. Because the optical electric field (with unit vector $\hat{e}$) is perpendicular to the z direction, $\alpha \propto |\hat{e} \cdot \vec{\mu}_{ba}|^2 \sim 0$ (11).

1. Ko H, et al. (2010) Ultrathin compound semiconductor on insulator layers for high-performance nanoscale transistors. *Nature* 468(7321):286–289.
2. Takei K, et al. (2011) Quantum confinement effects in nanoscale-thickness InAs membranes. *Nano Lett* 11(11):5008–5012.
3. Horng J, et al. (2011) Drude conductivity of Dirac fermions in graphene. *Phys Rev B* 83:165113.
4. Zhang Y, et al. (2009) Direct observation of a widely tunable bandgap in bilayer graphene. *Nature* 459(7248):820–823.
5. Nair RR, et al. (2008) Fine structure constant defines visual transparency of graphene. *Science* 320(5881):1308.
6. Takei K, et al. (2011) Benchmarking the performance of ultrathin body InAs-on-insulator transistors as a function of body thickness. *Appl Phys Lett* 99:103507.
7. Mead CA, et al. (1963) Fermi level position at semiconductor surfaces. *Phys Rev Lett* 10:471–472.
8. Olsson LÖ, et al. (1996) Charge accumulation at InAs surfaces. *Phys Rev Lett* 76(19): 3626–3629.
9. Bell GR, et al. (1997) Accumulation layer profiles at InAs polar surfaces. *Appl Phys Lett* 71:3688–3690.
10. Weber JR, et al. (2010) Intrinsic and extrinsic causes of electron accumulation layers on InAs surfaces. *Appl Phys Lett* 97:192106.
11. Chuang SL (2009) *Physics of Photonic Devices* (Wiley, Hoboken, NJ), 2nd Ed.

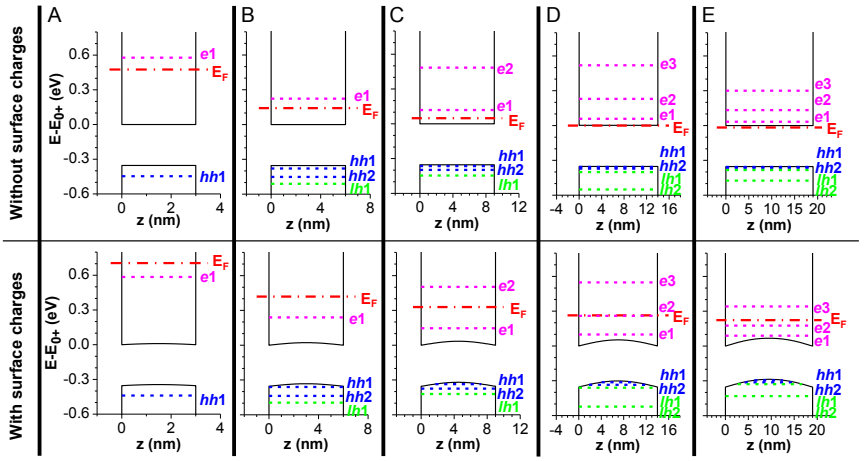

Fig. S1. Zoomed-in band alignments of CaF_2/InAs/air without and with surface charges ($N_S = 10^{12}$ cm^{-2}) for (*A*) 3-nm, (*B*) 6-nm, (*C*) 9-nm, (*D*) 14-nm, and (*E*) 19-nm InAs QMs. A bulk doping concentration of 2×10^{16} cm^{-3} was assumed.

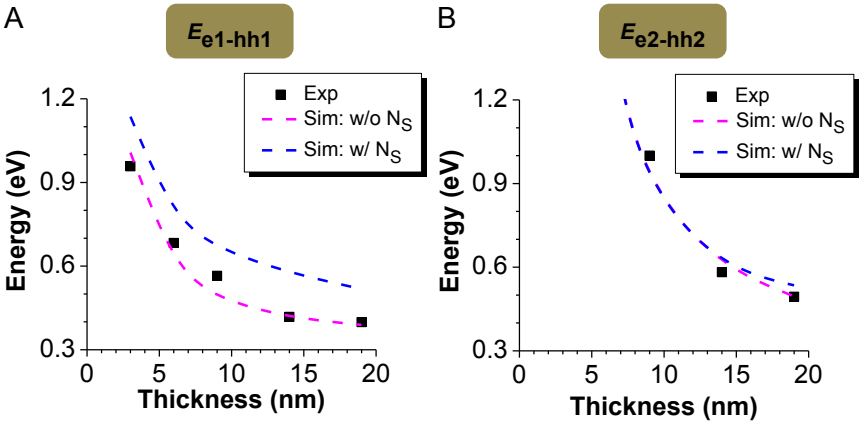

Fig. S2. Comparison of interband transition energies from experiment and modeling without and with surface accumulation charges for (*A*) $E_{e1\text{-}hh1}$ and (*B*) $E_{e2\text{-}hh2}$.